

Technical report

# **Development of a Neutron Field Monitoring System for the DT Neutron Generator Facility NESSA**

*Report submitted to the*

**Carl Trygger Foundation**

*as documentation for Grant*

**CTS 22:2218**

NESSA – Neutron Source at Uppsala

Göran Ericsson,

Sandipan Dawn, Linus Hägg, Stephan Pomp, Stefan Jarl-Holm and  
the NESSA team

Uppsala University

March, 2026

## Abstract

This report describes the procurement, installation and first tests of a neutron field monitoring system for the deuterium-tritium (DT) neutron generator facility NESSA at Uppsala University. The procurements were supported by a grant from the Carl Trygger Foundation. NESSA is under development at the Division of Applied Nuclear Physics, Uppsala University. At present, neutrons are produced by a generator on loan from SKB, a Sodern Genie 16 producing neutrons with energies around 14 MeV from  $d+t \rightarrow \alpha+n$  fusion reactions and capable of a maximum yield of about  $4.5 \cdot 10^8$  14-MeV neutrons per second.

The uFC monitoring system will provide reliable, continuous monitoring of the neutron flux at the facility, something that is essential for the scientific work and training programme at the facility. The monitoring system is based on two micro fission chambers (uFC) made by Centronic Ltd (UK), each with about 4 mg of active uranium deposit; specifically, Centronic type FC4A was selected for this application.

The fission chambers are based on  $^{235}\text{U}$  and  $^{238}\text{U}$  material, respectively, to differentiate between the fast and total neutron components of the field at different locations around the facility. As part of this project, the uFC were also equipped with charge-sensitive preamplifiers (Mesytec MPR-1), a high-speed digitizer (Teledyne SP Devices ADQ14), a low-voltage power supply (Mesytec,  $\pm 12$  V), a high-voltage supply (CAEN, up to  $\pm 5$  kV), and a large monitor for the NESSA beam control room. Together, these instruments form a complete pulse detection and data acquisition chain, thereby constituting a working neutron monitoring system ready for commissioning. This report explains the motivation behind each procurement choice and describes the key technical characteristics of each instrument as well as first experimental tests and some preliminary physics results.

Revision history:

- Original version of 2026-03-31.
- This version 2026-04-23: Section 6 was updated with new estimates of the detector efficiency and new data for the amount and mix of U in the deposit of the uFC.

## Contents

<b>1</b>	<b>Motivation .....</b>	<b>5</b>
<b>2</b>	<b>Overview of Fission Chambers and the Monitoring System.....</b>	<b>5</b>
<b>3</b>	<b>Procured Instruments and Technical Details .....</b>	<b>8</b>
3.1	Fission Chamber – Centronic FC4A ( $^{235}\text{U}$ ) .....	8
3.2	Charge-Sensitive Preamplifier – Mesytec MPR-1 .....	10
3.3	Voltage supplies .....	11
3.4	Low-Voltage Supply – Mesytec ( $\pm 12\text{ V}$ ) .....	11
3.5	High-Voltage Supply – CAEN (up to $\pm 5\text{ kV}$ , both polarities) .....	12
3.6	High-Speed Digitizer – Teledyne SP Devices ADQ14 .....	12
3.7	PXIe chassis and on-board control computer .....	12
<b>4</b>	<b>Signal Chain and System Integration .....</b>	<b>13</b>
<b>5</b>	<b>Experimental - irradiation campaign in February 2026.....</b>	<b>15</b>
5.1	Installation and commissioning .....	15
5.2	uFC data acquisition settings and signal properties .....	17
5.3	Event selection for Run 7 – uFC in CUP2 position .....	18
5.4	Run 7 – $^{235}\text{U}$ data selection and correction.....	18
5.5	Run 7 – $^{238}\text{U}$ data selection and correction.....	19
5.6	Event selection for Run 8 – uFC in FCIB position .....	19
5.7	Run 8 – $^{235}\text{U}$ data selection and correction.....	20
5.8	Run 8 – $^{238}\text{U}$ data selection and correction.....	20
5.9	uFC background data .....	21
5.10	Summary of count rate results .....	22
5.11	LaBr data .....	23
<b>6</b>	<b>Neutron transport calculations and estimated uFC count rates.....</b>	<b>23</b>
6.1	Estimate of the uFC detection efficiency .....	24
6.2	Calculation of the average (n,f) cross section and neutron flux at CUP2 and FCIB2... 26	
6.3	Calculation of uFC expected count rates at CUP2 and FCIB2 .....	28
<b>7</b>	<b>uFC count rates: Summary of results and discussion .....</b>	<b>28</b>
<b>8</b>	<b>Neutron generator source stability.....</b>	<b>29</b>
<b>9</b>	<b>Summary and conclusions.....</b>	<b>31</b>
<b>10</b>	<b>Acknowledgements .....</b>	<b>31</b>

**11 APPENDIX..... 32**

## 1 Motivation

The NESSA facility is a deuterium-tritium (DT) neutron generator facility under development at the Division of Applied Nuclear Physics, Dept of Physics and Astronomy, Uppsala University, Sweden. At present it is based on a Sodern Genie 16 DT generator, on long-term loan from the Swedish SKB company<sup>1</sup>. The generator uses fusion reactions between deuterons and tritons to produce neutrons with a yield of up to  $4.5 \cdot 10^8$  n/s in  $4\pi$  sr. The DT reaction,  $d + t \rightarrow {}^4\text{He} + n$ , produces neutrons centered at about 14.1 MeV. Work is ongoing to eventually complement the facility with a more powerful generator, capable of up to  $10^{10}$  n/s in  $4\pi$ . Applications currently under development at NESSA include neutron activation analysis, material irradiation studies, detector tests and nuclear data measurements. All these projects require a well characterized and continuously monitored neutron source and knowledge of the field's characteristics (energy resolved flux) at different positions around the facility. Changes in generator operating conditions such as ion current, target condition, gas pressure etc. can change the output flux over time during generator operations. Correcting for these variations after the fact is difficult and sometimes impossible. Therefore, a dedicated neutron flux monitoring system is essential. For the total (integrated) neutron yield over an operational period the most reliable monitoring method is normally based on activation samples. However, such a system gives no information on the variations of neutron flux during the experiments; for time resolved information fission chambers provide a well-tested, robust monitoring system.

Fission chambers are a standard choice for field monitoring in most neutron producing facilities, e.g. commercial fission nuclear power plants, experimental fusion devices and neutron generators of different source strengths. The well-known characteristics (energy dependent cross sections) of neutron-induced fission reactions (n,f) make detectors based on the  ${}^{235}\text{U}$  and  ${}^{238}\text{U}$  isotopes a good choice for providing an estimate of the absolute neutron flux, as well as information on the energy distribution of neutrons at different locations around the facility.

To suit the needs of the intended  $10^{10}$  n/s generator it was in the early days of NESSA developments decided to procure a micro fission chamber (uFC) of type FC4A from the UK-based company Centronic. With a total mass of about 4 mg of  ${}^{238}\text{U}$  (in the form of  $\text{U}_3\text{O}_8$ ) this was intended to monitor the high-energy component of the field and estimated to give reasonable fission rates (up to kHz) in positions close to the generator source point.

The present project, supported by the Carl Trygger foundation, was aimed at finalizing the neutron flux monitoring system, by procuring a second Centronic uFC, now based on  ${}^{235}\text{U}$ , and also procuring the auxiliary electrical and electronic equipment required for a complete monitoring system. This report describes the monitoring system set-up, the procurements and some first system tests and results.

## 2 Overview of Fission Chambers and the Monitoring System

Fission chambers are basically ordinary gas ionization chambers with the added component of a thin coating of an active fissile material (here  ${}^{235}\text{U}$  or  ${}^{238}\text{U}$ ) on one of the electrodes. When a

---

<sup>1</sup> Svensk Kärnbränslehantering AB, <https://skb.com/>. SKB is the Swedish company charged with managing Sweden's spend nuclear fuel.

neutron enters the active volume of uranium it may cause fission thereby releasing two highly charged, energetic fission fragments inside the detector. There is a high probability for at least one of the fission fragments to enter the fill gas and cause ionization. The ionization charges are collected on the electrodes under a bias voltage, producing a fast electrical pulse at the output. The count rate of these pulses is directly proportional to the neutron flux at the detector position. Fission chambers are well suited to high-intensity neutron environments because they tolerate gamma-ray backgrounds well and can handle a very wide range of flux levels. They can be constructed in various geometries and sizes; here small, so-called micro fission chambers (uFC) were used where their compact size provides flexibility and allows them to be placed close to the neutron production source point or within the facility's collimated neutron beam line without much disturbing the beam.

The NESSA monitoring system is based on a pair of uFC with different fissile coatings, one with  $^{235}\text{U}$  and one with  $^{238}\text{U}$ , both with the same geometry and each with a nominal amount of 4 mg of uranium. This arrangement provides a possibility to determine crude spectral information of the neutron field around the facility, based on the rather different energy-dependence of the (n,f) cross section for these isotopes, as shown in Figure 1. While  $^{238}\text{U}$  uFC is only sensitive to incoming neutrons with kinetic energy above about 1 MeV, the  $^{235}\text{U}$  (n,f) cross section is heavily biased towards low-energy neutrons. Note, however, that even for energies  $E_n > 1$  MeV, the  $^{235}\text{U}$  (n,f) cross section is about twice that of  $^{238}\text{U}$ . The uFC pair thus provides time-resolved neutron flux data, an estimate of the neutron fluence (independent from, e.g., the value estimated from activation foil data or from the electronic parameters of the generator) and in addition gives information about the spectral composition of the neutron field. This is essential information for many applications since even a nominally mono-energetic 14 MeV source will produce a large component of scattered, energy down-graded neutrons in the surrounding environment.

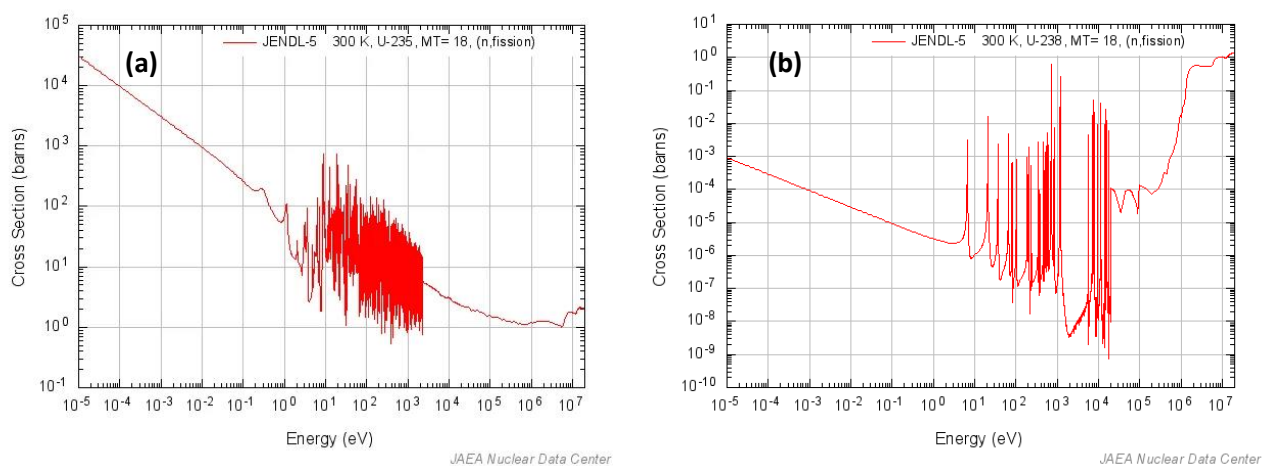


Figure 1. (a) Cross section for the (n, fission) reaction in  $^{235}\text{U}$ . (b) Cross section for the (n, fission) reaction in  $^{238}\text{U}$ . From JAEA web-based data tool2, using JEMDL-5 data set. Both plots for incoming neutron energies between 10-5 and 107 eV. Note the difference in vertical scale.

The signal from the uFC must be amplified, digitized, and recorded, in order to give the intended

<sup>2</sup> [https://www.ndc.jaea.go.jp/ENDF\\_Graph/](https://www.ndc.jaea.go.jp/ENDF_Graph/)

time-resolved flux during an experiment. A sketch of the required components of the complete monitoring system is shown in Figure 2. Further details are given in the next section.

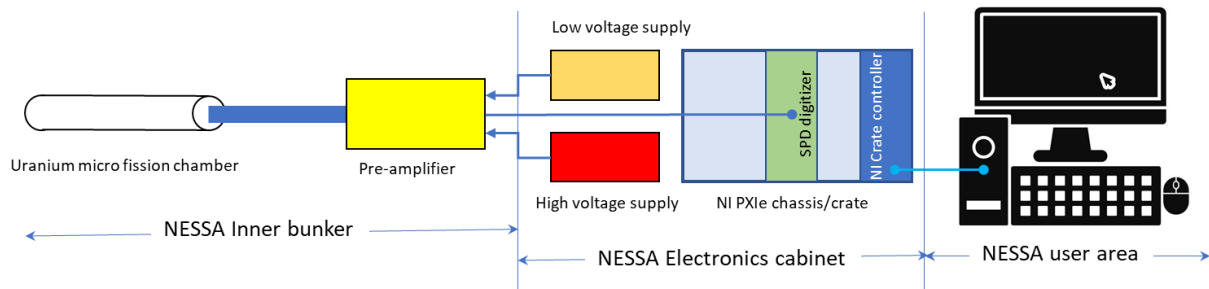


Figure 2. Schematic diagram of the electronic units required for operations and data acquisition of one of the micro fission chambers in the NESSA flux monitoring system. Both uFC had identical set-ups. For details see text.

One type the information that can be gained from fission chamber data is the so-called pulse height spectrum. This is basically a histogram of the collected charge from individual fission events in the detector; pulse height is here represented by the integrated charge of the fission event (see Section 5.2 for further details).

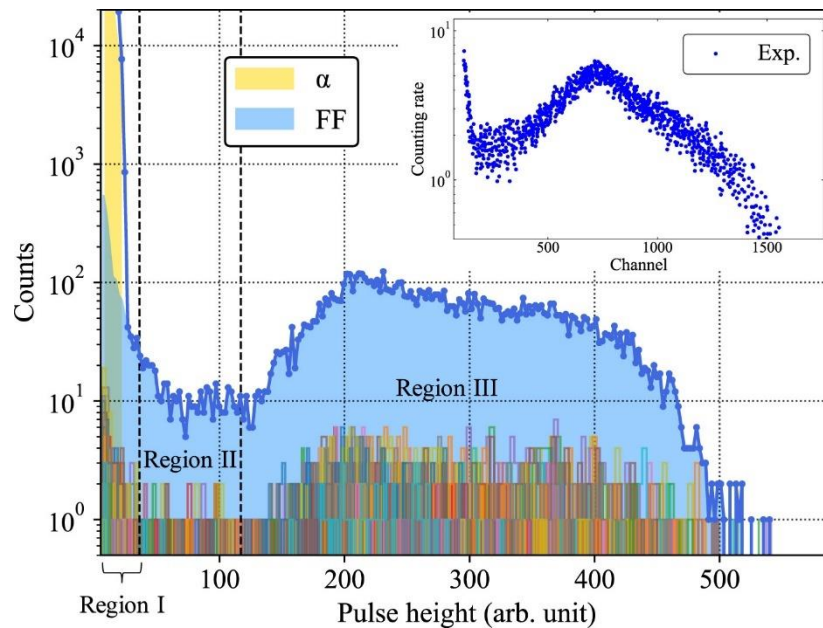


Figure 3. Simulated and experimental results obtained for the FC4A uFC by Yang, *et al.* The large panel shows their simulation results. The small insert shows their experimentally measured pulse height spectrum (histogram).

Many studies have been devoted to this aspect of fission chamber information, both experimental and modelling; of particular interest for the data analysis described later in this report is the study by Yang *et al.*<sup>3</sup> They have studied, both in simulations and with measurements, the performance of the Centronic FC4A uFC, exactly the type used in our monitoring system; in Figure 3 is shown their calculated and measured pulse height spectrum. From the simulations we can observe a broad “mountain” (Region III) of data due to fission events. At lower pulse heights we see a flat region (Region II), at an amplitude about ten times

<sup>3</sup> Yang *et al.* Nucl. Instr. Meth. A1076 (2025) 170441

lower than the peak of Region III, also containing mostly fission events. Below this region the simulated histogram rises sharply. This rise is mainly due to alpha particle events in the detector; Uranium has a natural alpha decay, and these alpha particles may enter the detectors gas-filled volume and give rise to a signal of low pulse height. But it also contains an appreciable component of fission events, as indicated by the blue histogram below the yellow alpha particle data. In the analysis presented later in this report we have used the results of Yang et al., to estimate the total number of neutron-induced fission events (absolute). To be specific, we have assumed a uniform level of events below the discriminator threshold, all the way down to 0 pulse height. By doing this we can assess the absolute neutron flux at the detector position.

### 3 Procured Instruments and Technical Details

#### 3.1 Fission Chamber – Centronic FC4A ( $^{235}\text{U}$ )

As part of this project, we have procured one fission chambers of type FC4A coated with  $^{235}\text{U}$ , manufactured by Centronic Ltd (UK) (now Exosens<sup>4</sup>). A second FC4A uFC with  $^{238}\text{U}$  was already available from a previous procurement. Both uFC have the same miniature design (Figure 4) which is well established for reactor physics and accelerator facility applications.

The FC4A is a compact cylindrical, axis symmetric detector built specifically for flux monitoring in confined geometries. The body and electrodes are made from a nickel-iron-cobalt alloy chosen for its gas-sealing properties. The chamber is filled with argon plus 2% nitrogen at 75 psi (absolute). The fissile coating is applied as uranium oxide ( $\text{U}_3\text{O}_8$ ) with a nominal thickness of  $1 \text{ mg/cm}^2$  (of uranium) to the  $4 \text{ cm}^2$  surface of the outer cathode. Nominal detector parameters are further given in Table 1.

We chose the  $^{235}\text{U}$  FC4A primarily to complement the existing  $^{238}\text{U}$  chamber, which, in turn, was selected for its compact size and suitable performance. The manufacturer's stated neutron sensitivities of  $3 \times 10^{-3} \text{ cps nv}^{-1}$  for the  $^{235}\text{U}$  chamber in a room-temperature thermal flux and  $6.94 \times 10^{-6} \text{ cps nv}^{-1}$  for in a mono-energetic 2.5 MeV n flux (see footnote below) gives reasonable count rates within the operating range of our (intended) DT generators, albeit a bit on the low side for the  $5 \cdot 10^8 \text{ n/s}$  Sodern generator (further details below). The rated uFC lifetime of  $10^{16} \text{ nvt}$  is more than sufficient for the planned operational period of NESSA.

At present, the two uFC are mounted side-by-side in a plastic holder (Figure 5) to provide a degree of reproducibility in the experimental tests. The holder can be mounted at different locations around the NESSA facility, for comparison with neutron transport calculation, e.g. those done as part of the facility's safety case, and to map the field for experiments.

The two uFC were tested in various hardware configurations in late 2025, partly to determine suitable choices for pre-amplifiers, HV and LV units etc.; this preliminary work resulted in the procurements described in this report.

---

<sup>4</sup> <https://www.exosens.com/products/fission-chambers-core-use>

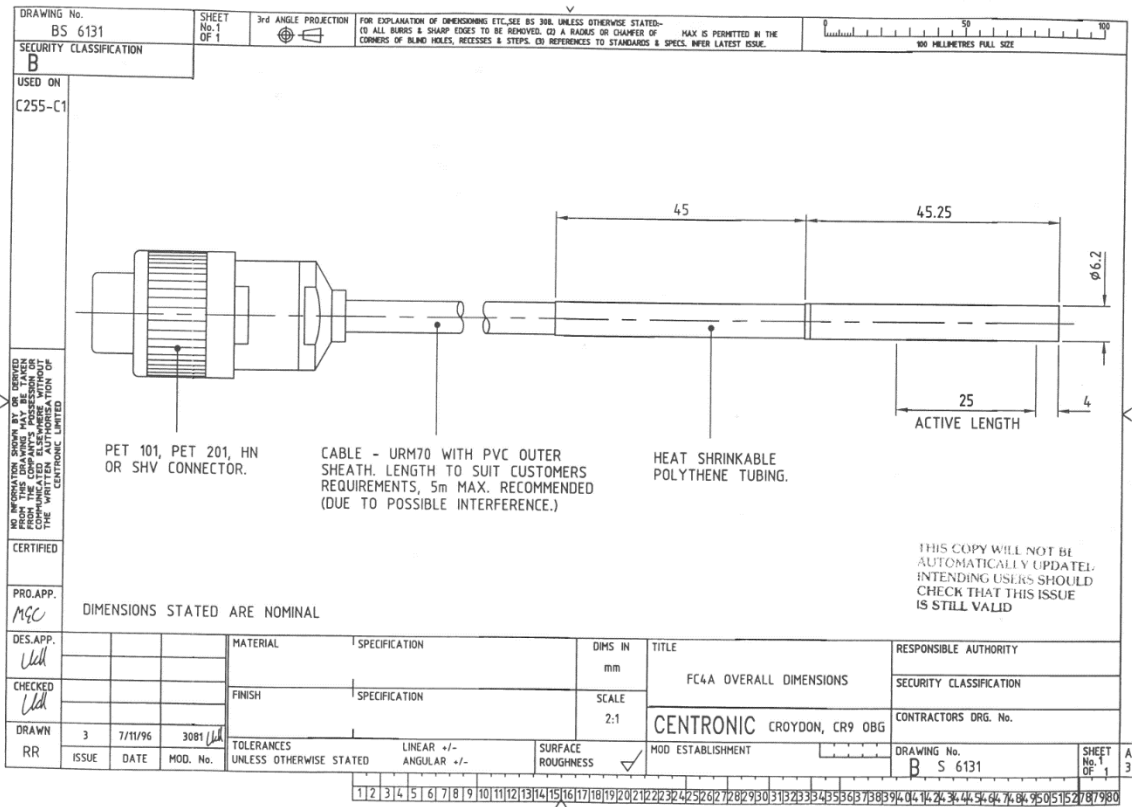


Figure 4. Schematic drawing of the FC4A uFC and associated cable with HN connector attached, courtesy of Centronic Ltd.



Figure 5. The pair of uFC placed in a simple holder made of thin plastic components on a thin Al base plate. Here the pair is mounted on the wall of the NESSA inner bunker, in a position known as the FC-IB. See Section 5 for further details on the measurements in this position.

**Table 1. Electrical and performance parameters of the Centronic FC4A fission chamber. Values quoted for  $^{235}\text{U}$  coating at  $1 \text{ mg cm}^{-2}$  density.**

Parameter	Value
Fissile materials available	$^{232}\text{Th}$ , $^{235}\text{U}$ , $^{238}\text{U}$
Coating density (standard)	$1 \text{ mg cm}^{-2}$
Coating form	Uranium oxide, $\text{U}_3\text{O}_8$
Fill gas	Argon + 2% Nitrogen
Fill pressure	75 psi (absolute)
Typical operating voltage	500 V inter-electrode voltage (maximum 1000 V)
Neutron sensitivity ( $^{235}\text{U}$ )	$3 \times 10^{-3} \text{ cps nv}^{-1}$
Neutron flux range	$3 \times 10^3$ to $3 \times 10^7 \text{ nv}$
Amplifier charge sensitivity	$6 \times 10^{-14} \text{ C}$
Current pulse amplitude	$> 1.2 \times 10^{-6} \text{ A}$ (90% of pulses)
Maximum integrated neutron fluence	$10^{16} \text{ nvt}$
Maximum operating temperature	$80^\circ\text{C}$

### 3.2 Charge-Sensitive Preamplifier – Mesytec MPR-1

The fission chamber signals need to be amplified before they can be further handled by the data acquisition system. After initial tests of the  $^{238}\text{U}$  chamber with a few different pre-amplifiers (from CAEN, Ortec and Mesytec), we selected the Mesytec MPR-1, a single-channel charge-integrating preamplifier, for this system. Two such units, one for each uFC, were procured as part of the project (Figure 6).



*Figure 6. The Mesytec MPR-1 preamplifier (yellow box) installed in the NESSA inner bunker. The pre-amp is kept close to the neutron generator to keep the cable length to the fission chamber as short as possible.*

The MPR-1 provides two outputs, each driving a terminated  $50 \Omega$  cable; one provides a fast

timing signal, the other provides a slower signal intended for energy determination. The two outputs can be set to the same polarity, or one can be configured as a timing filter output – useful when a trigger timing is used alongside the energy information. A front-panel switch changes the sensitivity by a factor of five, which is handy when working with different detector geometries or coating densities.

The MPR-1 integrates the charge from each fission pulse and converts it to a voltage step with a rise time below 12 ns at low detector capacitance. Signal and bias high-voltage is connected from the pre-amp to the detector through a common co-ax cable. The signal is filtered out by the unit's built-in T-filter (RCR) arrangement with a 10 M $\Omega$  input resistor and a 4.7 nF capacitor, which cleanly separates the detector bias (nominally 500V) from the detector signal (few V at most). Technical data for MPR-1 in Table 2.

**Table 2. Technical parameters of the Mesytec MPR-1 charge-sensitive preamplifier.**

Parameter	Value
Type	Charge-integrating, single channel
Input	ESD-protected; positive and negative charge
Bias voltage (with SHV connectors)	up to $\pm 3000$ V
Open-loop gain	typically 60000 at 1 pF integration capacity
Signal risetime (0 pF load)	<12 ns
Signal risetime (100 pF load)	25 ns
Output swing (unterminated)	0 to $\pm 8$ V Decay time 100 $\mu$ s
Temperature drift	< $\pm 50$ ppm/ $^{\circ}$ C
Nonlinearity	<50 ppm
Timing filter time constant	33 ns
Power supply requirement	+12 V at 40 mA; -12 V at 30 mA
Dimensions	60 $\times$ 143 $\times$ 30 mm

### 3.3 Voltage supplies

Several units in the system require low- and/or high voltage bias for proper operations. This includes the uFC which need a few hundred volts bias voltage over the ionization chamber's electrodes (here we used a bias voltage of 500 V) and the pre-amplifiers which typically need a combination of  $\pm 6$ V and  $\pm 12$ V for their electronic components. It should be noted that both high and low voltage is supplied to inputs on the Mesytec pre-amp unit, which in turn sends the bias high voltage to the detector.

Two power supplies have been procured to support the detector operations and data acquisition chain as further described below.

### 3.4 Low-Voltage Supply – Mesytec ( $\pm 12$ V)

The MPR-1 pre-amplifier requires a stable, low-noise supply of +12 V at 40 mA and -12 V at 30 mA. For this purpose, a Mesytec 4-channel unit was procured. This supply is well matched to the MPR-1 and connects via a standard Lemo-to-SubD-9 cable supplied with the pre-

amplifier. Such a matching purpose-built supply from the same supplier as the pre-amplifier is a preferred solution over a more general bench unit since such supplies typically carry more ripple and switching noise than a charge-sensitive amplifier can tolerate at its input stage.

### 3.5 High-Voltage Supply – CAEN (up to $\pm 5$ kV, both polarities)

The fission chambers need a well-regulated bias voltage between their anode and cathode to sweep ionization charges from the gas volume efficiently. The CAEN high-voltage supply, rated to  $\pm 5$  kV with both polarities available, provides this bias. The FC4A operates typically at 500 V with an absolute maximum of 1000 V, so the CAEN supply has ample headroom. The dual-polarity capability is useful when working with different detector configurations.

For this purpose, a 4-channel HV supply capable of  $\pm 5000$ V was procured (CAEN). The supply is connected to the NESSA control room computer via standard network cabling. Software provided with the unit gives the possibility to set HV levels as well as ramp-up and ramp-down time constants (V/s).

### 3.6 High-Speed Digitizer – Teledyne SP Devices ADQ14

The energy output signals of the MPR-1 are sent to a Teledyne SP Devices ADQ14 waveform digitizer. The ADQ14 has four analog input channels, a sampling rate of up to 1 GSPS per channel, and 14-bit vertical (amplitude) resolution. For this monitoring system, the most important feature is the capability to capture the complete pulse shape of each fission event in real time, which allows for further off-line pulse analysis and pulse shape discrimination.

**Table 3. Selected specifications of the Teledyne SP Devices ADQ14 waveform digitizer.**

Parameter	Value
Number of analog channels	Up to 4
Maximum sample rate	1 GSPS per channel
Vertical resolution	14 bits
Analog bandwidth (DC-coupled)	up to 1.2 GHz
On-board data memory	2 GBytes
Maximum data transfer rate (PXIe)	up to 3.2 GBytes/s
Data interfaces	PXIe, PCIe, USB3.0, MTCA.4, 10 GbE
Trigger modes	Internal and external
FPGA	Open, programmable (development kit required)
Software supported	Windows, Linux; C/C++, Python, MATLAB, LabVIEW

The digitizer is PXI express (PXIe) type, a common form for modular data acquisition electronic in scientific and product testing environments. It is installed in a dedicated PXIe chassis (crate) with an on-board control computer (see next Section). Technical details in Table 3.

### 3.7 PXIe chassis and on-board control computer

The SPD digitizer is housed in a PXIe chassis (crate) procured from National Instruments. On

its back plane, the chassis provides the necessary low-voltage power for the digitizer electronics and a data bus to transfer the digitizer information to the control computer (and further, possibly after some data reduction, to long term storage). In this application we have procured a National Instruments on-board control computer, installed in the same PXIe chassis as the digitizer, to handle the data acquisition software and directly receive the digitizer data. The on-board computer is connected to a common screen, mouse and keyboard in the NESSA control room and has a network connection to the remote University data storage facilities.

We have developed an in-house Python-based computer code to acquire, store, plot, and analyze the digitized fission chamber data, with a graphical user interface also providing real time neutron rate monitoring in the NESSA “control room” (at present a user area just outside of the NESSA radiation protection bunker).

## 4 Signal Chain and System Integration

Except for the pre-amplifier, which is placed close to the actual uFC detectors in the NESSA inner bunker, the electronic units of the uFC signal chain are placed in a standard equipment cabinet just outside the NESSA bunker, in close connection to the facility’s “control room” as shown in Figure 7.

The signal chain from detector to data storage is schematically outlined in Figure 1. Each fission chamber is biased from the high-voltage supply via the MPR-1 preamplifier. When a neutron induces fission in the chamber, the ionization of the detector fill gas may occur and the released charge is collected at the electrodes and appears as a fast current pulse at the preamplifier input. The MPR-1 pre-amplifier integrates this charge and produces a shaped voltage pulse at its output. This pulse is transferred by RG58 coaxial cable (via a patch panel in the NESSA inner bunker) to the SPD ADQ14 digitizer in the NI PXIe chassis.

The digitizer samples the incoming voltage waveform every ns (1 GHz sampling frequency) with 14 bit (16384 codes) vertical resolution. The digitizer has 4 independent input channels with 0.5 V<sub>pp</sub> input range, is DC coupled with programmable DC offset and has a 2 GByte onboard memory for temporary storage of acquired data.

Each fission chamber connects to a separate input of the ADQ14, allowing fully parallel acquisition with no dead time between the two detectors. The unit offers a variety of trigger modes; for this work a simple level trigger scheme was implemented. For each triggered readout, the trigger time stamp and a record of 70000 sampled voltage values (70 μs of data) were stored and transferred to control computer. The ADQ14’s multi-channel synchronization keeps timestamps from all channels aligned to the same clock, which is important for any correlation analysis between the detectors. After some initial analysis (see below) the records were reduced by a factor 1000 in order to save storage space.

For the NESSA real-time neutron rate monitoring system, collected events are classified as either noise or real events based on pulse shape. Real events are counted towards the number of digitized events per unit time per uFC to get an initial rough indication of the total (<sup>235</sup>U) and fast (<sup>238</sup>U) neutron rates. These data are displayed in the NESSA control room, to which a large monitor has been procured as part of this project. The in-house Python acquisition

software displays the real-time flux data to this screen, giving operators a continuous view of beam conditions during experiments.

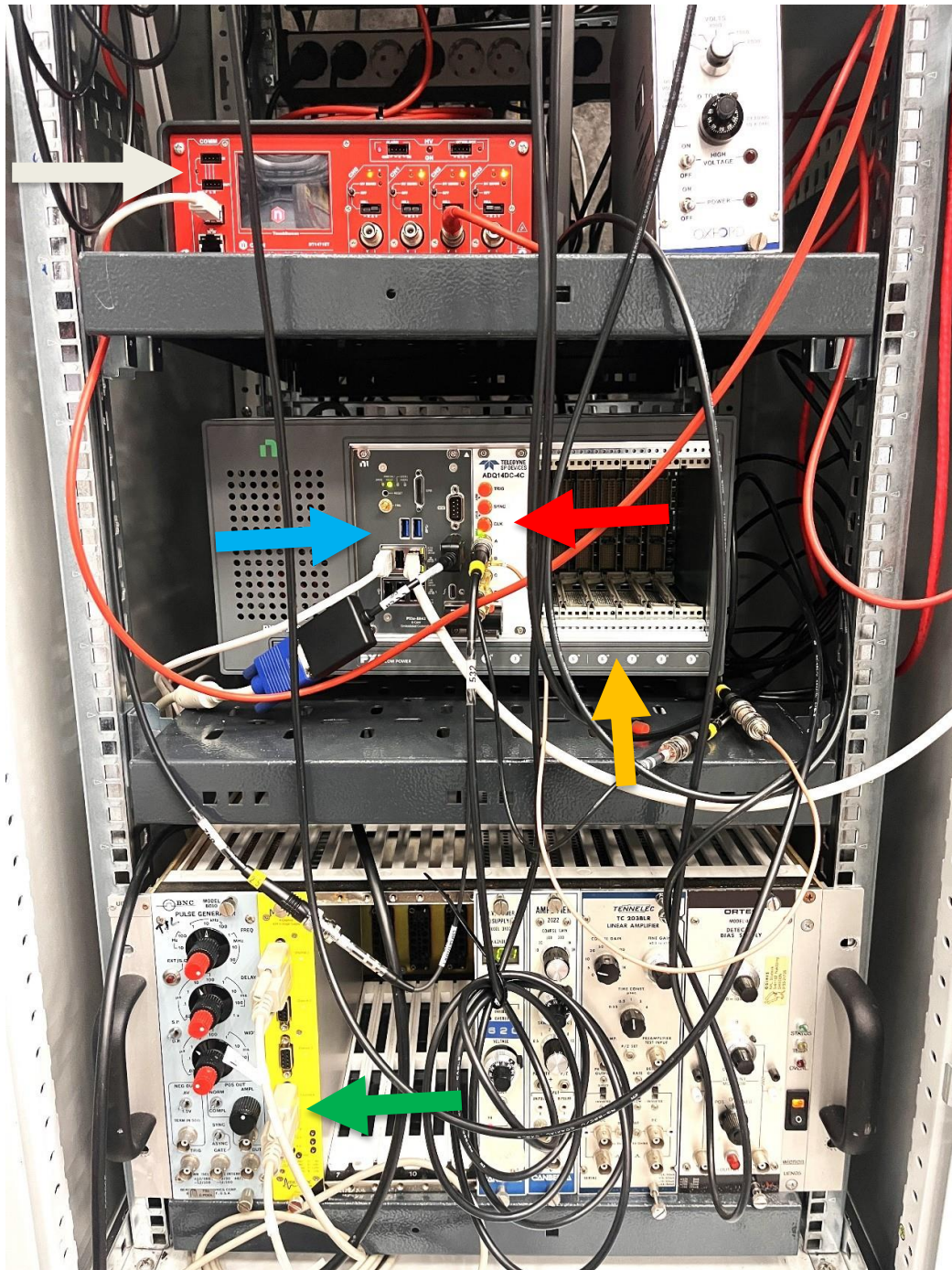


*Figure 7. Electronics units for the uFC monitoring system were installed in a dedicated cabinet just outside of the NESSA radiation bunker. The relevant units are indicated by colored arrows. CAEN high-voltage supply (off white), NI PXIe chassis (orange), NI onboard control computer (light blue), SPD ADQ14 digitizer (red), and Mesytec low-voltage power supply (green).*

## 5 Experimental - irradiation campaign in February 2026

### 5.1 Installation and commissioning

The new uFC monitoring system was installed and commissioned at the NESSA facility in a series of long-term measurements in February 2026. For these measurements the two uFC were always used as a pair, mounted in the plastic holder as shown in Figure 5 and Figure 8.

The purpose of these experiments was three-fold:

- 1) Commission the new uFC neutron rate monitoring system,
- 2) Make measurements in two positions for which MCNP neutron transport calculations were done as part of the NESSA safety case to the Swedish Radiation Safety Agency (SSM); compare measurements with calculations,
- 3) Make irradiations of activation samples of In and Nb to estimate the absolute neutron yield of the Genie16; compare to nominal values from the manufacturer and earlier calibrations performed at Lund University.

To this end, three data taking runs were conducted in the period Mon. Febr. 16 to Wedn. Febr. 18, 2026. Some of the operating parameters for these runs are summarized in Table 4.

**Table 4. Measurement campaign information Feb 16-18, 2026.**

Date, start time (h:m:s)	Local run #	Data acquisition time (h:m:s)	Average neutron rate (n/s) (*)	uFC position	Comment
2026-02-16 14:15:45	7	4:0:0 14400 s	$4.4 \cdot 10^8$	CUP2	Small variation in NG operating parameters for the first few minutes
2026-02-17 13:39:00	8	19:34:16 (**) 70456 s	$1.8 \cdot 10^8$	FCIB2	Lower operating settings than for Run 7; Stable for the whole run
2026-02-18 13:55:47	Background	2:59:59 10799 s	0	FCIB2	Neutron generator switched off

(\*) Based on a rate calibration performed previously at Lund University and the recorded electrical operating parameters for each run.

(\*\*) Run 8 was intended to extend over 24 hrs, but a crash of the data acquisition system terminated the run prematurely.

Photos of the uFC installed in the two measurement positions are shown in Figure 8.

In panel Figure 8c is shown the uFC pair (and activation samples) installed for the 4-hour run on Monday 16 Febr. Here the aim was to measure in the so-called Close User Position #2

(CUP2)<sup>5</sup> which refers to the closest available position to the Genie16 neutron generator source point (Ti target). With a nominal outer radius of 35 mm for the Genie16, and some additional distance due to the holder (2 mm) and the radius of the uFC (3 mm) the total average distance of the active U material in the CUP2 to the center of the neutron emission target is 40 mm.

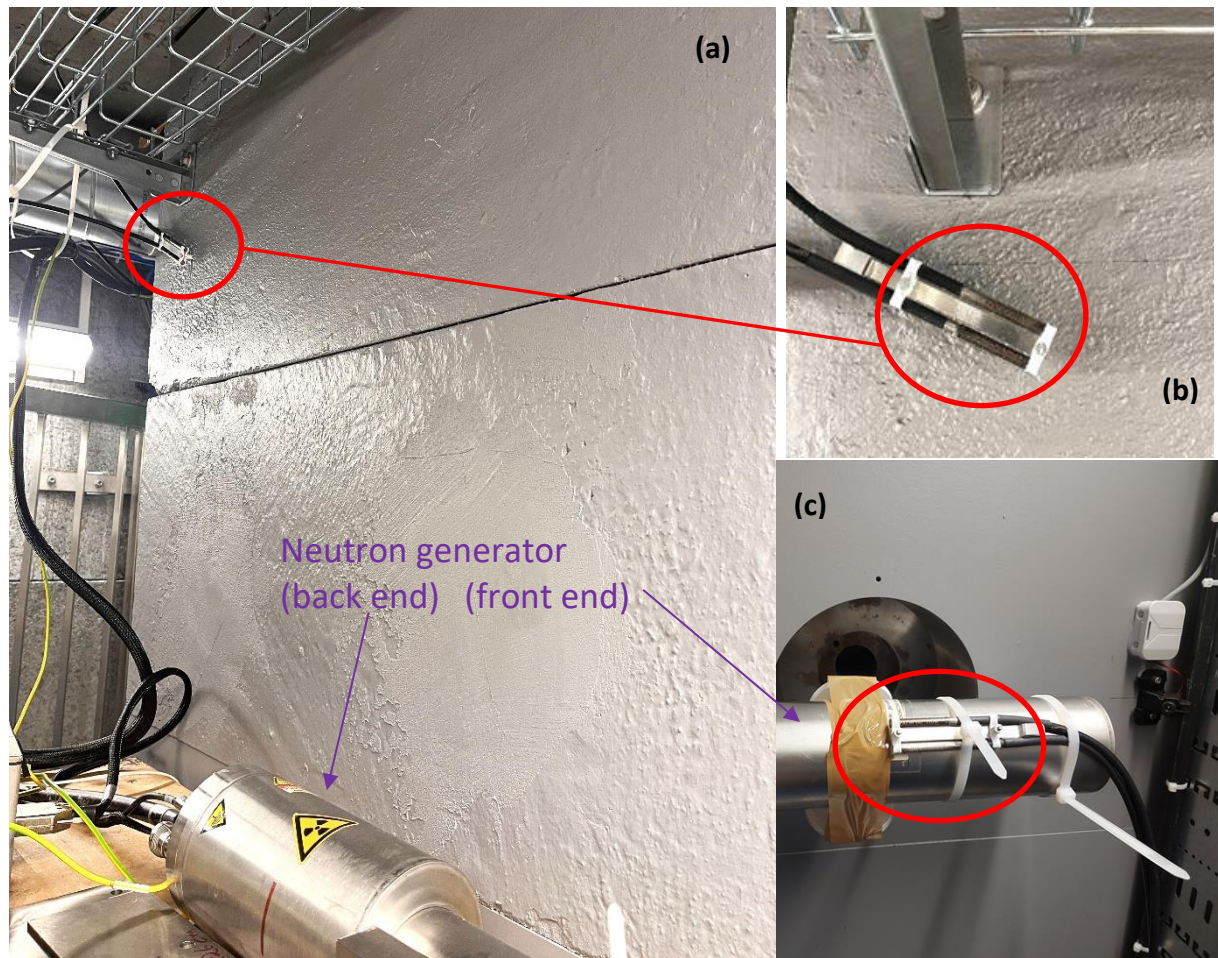


*Figure 8. Three photos of the installation of the uFC pair (indicated by red circles) in the NESSA inner bunker for long term measurements. (a) uFC in the so-called FC-IB position with the back end of the neutron generator visible in the lower part of the photo. (b) Detail of the uFC pair in the FCIB2 position. (c) The uFC pair installed in the so-called Close User Position #2, provisionally attached to the neutron generator tube by tie wrap plastic bands. Here is also seen the two plastic cups containing the activation samples, partly hidden behind the tube and provisionally attached by brown tape.*

In panel Figure 8a is shown the uFC pair installed for the 20-hour run Tue. Feb.17 – Wed. Feb. 18. This is the so-called Fission Chamber Inner Bunker (FCIB2) position, about 130 cm from the generator source point. The detectors were mounted to point towards the generator source point, in order to give a symmetric situation where both uFC receive the same neutron flux.

Two scintillator detectors, one with LaBr and one with NaI as scintillating material, were also used in these experiments to gain further information on the time evolution of the neutron rate

<sup>5</sup> The identification CUP2 is to distinguish the closest user position for the present Genie16 generator from an alternative position at 17 mm from the neutron source point, valid for another type of DT generator and used in MCNP calculations later in this report.

from the generator. In particular the LaBr-based detector provided useful data, and it is used in the evaluation below. The signal from each scintillator was fed into a separate input of the ADQ14 digitizer.

## 5.2 uFC data acquisition settings and signal properties

An example of the data recorded for one of the uFC is shown in Figure 9. This is actually the full set of data recorded by the  $^{238}\text{U}$  uFC over the 70456 seconds of Run 8, when the detector was placed in the FCIB2 position. This position, at about 130 cm from the neutron source point, in combination with the small amount of fissile material and the low sensitivity of the  $^{238}\text{U}$  chamber to low-energy (scattered) neutrons resulted in a quite low count rate, with only 1000 events<sup>6</sup> recorded for the full Run 8.

In Figure 9a is shown the pulse shapes of 776 events selected as good fission events. The pulses display the expected base line at around 15000 codes and then a sharp drop at the time when the trigger condition is fulfilled. Then there is a long, slow decay of the pulse until the end of the record. The pulse shapes are mainly given by the action of the pre-amplifier, which in this set-up gives very long pulse decay times. The rounded shape of the pulses after the trigger is not typically expected for this detector-preamplifier combination and could be the result of some damage sustained by the detector when operated at too high HV in some early tests.

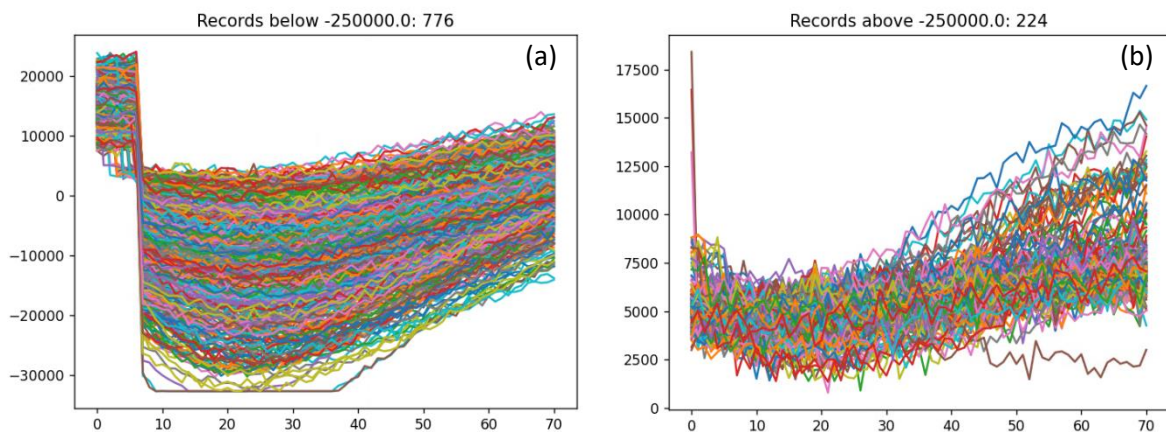


Figure 9. Pulse shapes of the events from the  $^{238}\text{U}$  uFC in Run 8 with the detector placed in the FC-IB position. The vertical scale is in digitizer codes (with a 4x scale factor applied). The horizontal scale is in  $\mu\text{s}$ . (a) Pulse shapes of all 776 events selected as good fission events. (b) Pulse shapes of the 224 events discarded as non-fission events.

As can be seen in Figure 9, pulses from the uFC are of negative polarity. A level trigger at 2500 codes (absolute) was set, meaning that in order to trigger a read-out, at least one sample of an event had to have a code value lower than this number. The acquisition was set to sample the pulses over 70  $\mu\text{s}$ , including a pre-trigger period of 7  $\mu\text{s}$  to evaluate the level of the base line for each individual pulse. As seen in panel (a), base lines of different events vary considerably, so in order to properly calculate the integrated charge (sum of codes) of each event an individual average base line had to be calculated and subtracted from each amplitude code value for the

<sup>6</sup> This number is due to the settings of the acquisition program, which only writes data to storage when a buffer of 100 events is filled. At the time of the crash of the acquisition system, exactly 10 such buffers had been stored.

event.

In what follows, most of the data evaluation and selection will be done based on the pulse height of individual events. Pulse height here means the summed codes values of a triggered event after subtraction of its average base line level has been performed.

### 5.3 Event selection for Run 7 – uFC in CUP2 position

Data acquisition Run 7 had the two uFC installed in the close user position (CUP2) for the Sodern generator, i.e., on the side of the tube at about 40 mm from the neutron source point; the run lasted for 4 hrs. See Figure 8c.

#### 5.3.1 Run 7 – $^{235}\text{U}$ data selection and correction

The pulse height spectrum (base line subtracted) for all recorded events in the  $^{235}\text{U}$  uFC for Run 7 is shown in Figure 10a. Here one can observe a sharp peak at about -12000 integrated codes, a sharp dip in the distribution at the position indicated by a red line and a broad distribution of events to the right of the red line. We identify the peak at -12000 codes as a data pedestal (background due to events without a proper base line), the dip at the red line as an indication of the acquisition trigger threshold and the broad distribution as due to good fission events above the threshold. It should be noted that since base line subtraction is performed for each individual event, the zero-point in the pulse height scale is expected to be at pulse height integral 0.

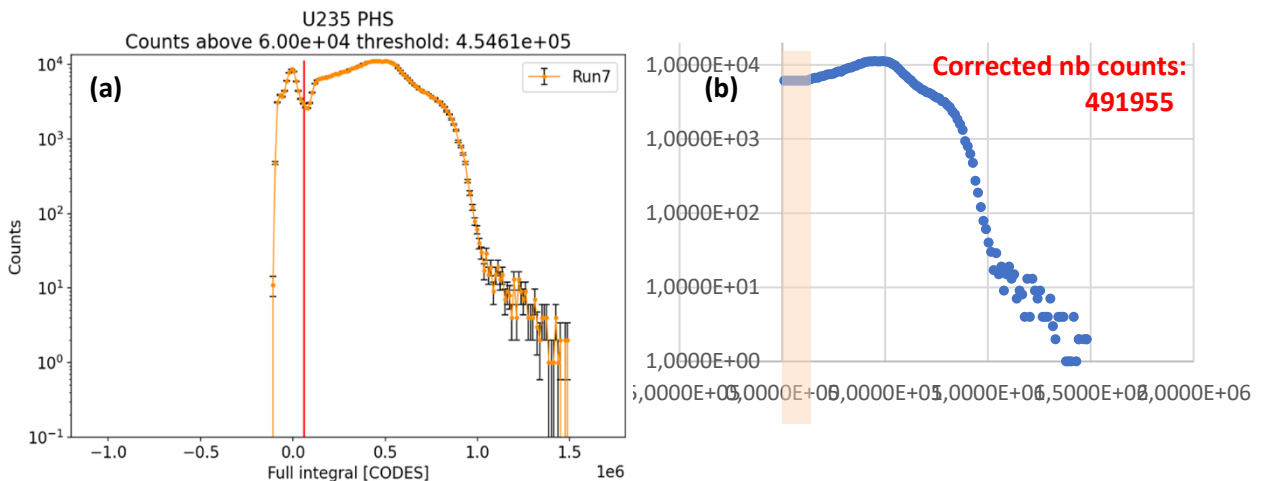


Figure 10. Data from the  $^{235}\text{U}$  uFC in Run 7. Note that pulse shapes have been inverted to form (mostly) positive pulse height integrals. Logarithmic vertical scale. (a) Pulse height spectrum of the full set of recorded events. The red line designates a preliminary software threshold used for the real time monitoring system. (b) The corrected data set after removal of the low-integral peak (just below 0 integral in panel (a)) and addition of events assumed lost below the acquisition hardware threshold in the region marked by the orange band. Text for details.

The red line indicates a software threshold, used as a rough separation of “good” fission events from background based on pulse height alone. This selection gave a total of 454610 good fission events (i.e., events to the right of the red line). It is also the basis for the estimated neutron rate in the on-line monitoring system.

Panel b shows the pulse height spectrum after subtraction of the pedestal peak and addition of events below the hardware discrimination threshold. The simulations presented in Figure 3

suggest that there is a Region II of essentially uniform event distribution extending towards low pulse heights; we have therefore added events according to a uniform distribution from the discriminator threshold down to pulse height integral 0; this region is marked by an orange band in the figure. Summing up all events in the resulting spectrum gives **491955** good fission events.

### 5.3.2 Run 7 – $^{238}\text{U}$ data selection and correction

The pulse height spectrum (base line subtracted) for all recorded events in the  $^{238}\text{U}$  uFC for Run 7 is shown in Figure 11a. A pedestal is seen at a pulse height of about  $-10^5$  integrated codes, and a broad peak around pulse height  $10^6$  integrated codes. In this case there is some uncertainty as to where the hardware discriminator threshold is positioned the data, with a best guess at  $3 \cdot 10^5$  integrated codes where a knee in the distribution can be observed. Following the recipe from the previous section, we fill out all bins below the assumed threshold with a uniform event distribution, as seen in panel (b). We now assume that all data above pulse height integral value 0 represent good fission events and simply sum up the number of entries in the histogram for pulse height integrals larger than 0. The estimated number of good fission events is **146852**.

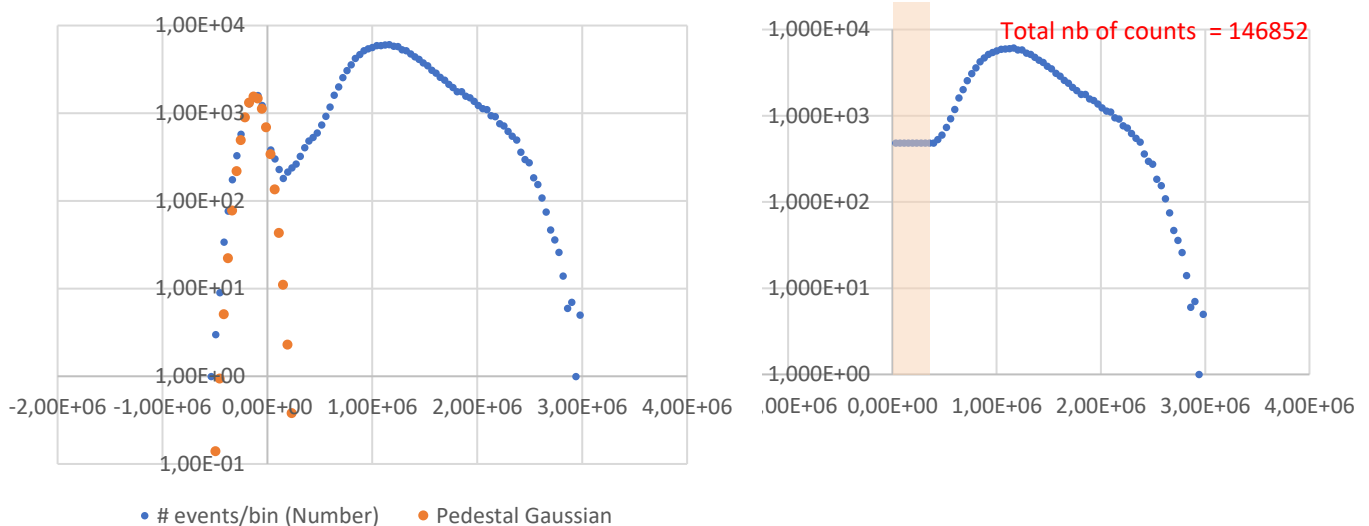


Figure 11. Data from the  $^{238}\text{U}$  uFC in Run 7 and from the 4-hr background measurement.

Horizontal scale in integrated codes. (a) Histogram of  $^{238}\text{U}$  uFC data in blue dots, scaled Background run data in orange dots. Logarithmic vertical scale. (b) Histogram of corrected data after the removal of the pedestal events and addition of a uniform distribution below the assumed discriminator threshold, as marked by the orange band.

### 5.4 Event selection for Run 8 – uFC in FCIB2 position

Data acquisition Run 8 had the two uFC installed close to the so-called Fission Chamber Inner Bunker (FCIB2) position. A position close to this, FCIB1 had been used in MCNP calculations as a possible permanent location of monitoring fission chambers in the NESSA inner bunker. FCIB1 is situated on the bunker wall, at 135 cm from the neutron source point. For practical reasons the pair of uFC could not be placed at exactly this distance from the source point but had to be shifted slightly closer to the generator. The experiment Run 8 was therefore conducted with the uFC pair installed in FCIB2 at about 130 cm from the neutron source point; it lasted for about 20 hours, differing a bit between detectors due to a crash of the data acquisition system and the peculiarities of how data is written from the on-board computer to permanent storage.

#### 5.4.1 Run 8 – $^{235}\text{U}$ data selection and correction

Corrected pulse height spectra (base line subtracted) for events from the  $^{235}\text{U}$  uFC for Run 8 is shown in Figure 12. In panel (a) is shown the spectrum where a model of the pedestal (again at -12000 codes) has been subtracted from the full spectrum. This enhances the sharp action of the assumed hardware threshold, and the remaining spectrum falls to a low point of almost 0 counts close to pulse height 0. We take this to indicate that data in the orange region in panel (b) is affected by the discriminator action and assume that the actual data follows a uniform distribution down to 0 pulse height. When summing up all counts above pulse height 0 in panel (b) we obtain a corrected number of counts of **162236**.

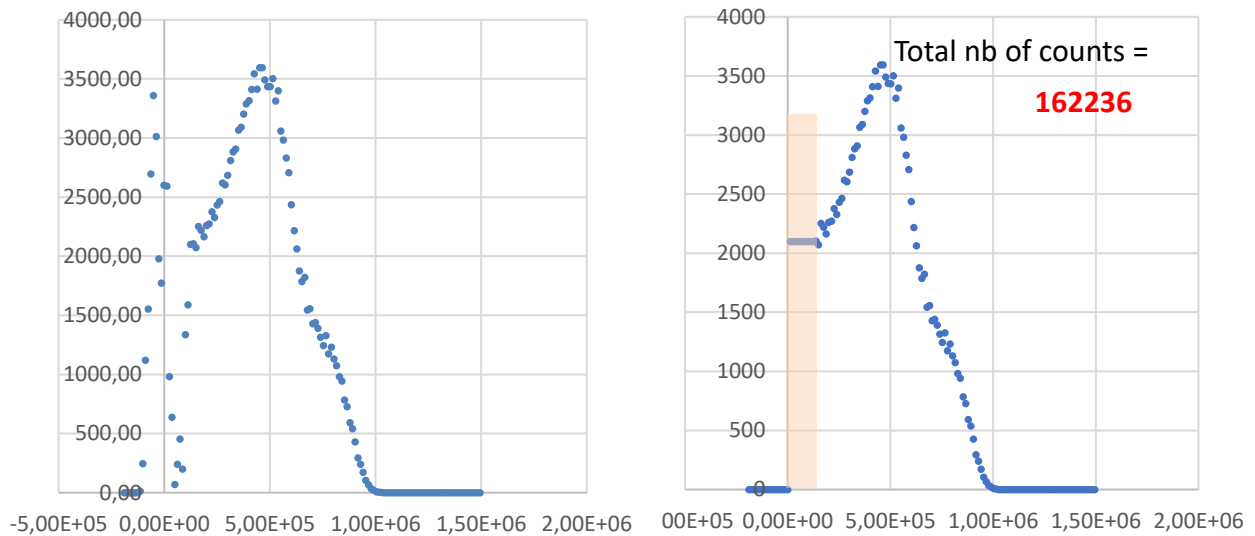


Figure 12. Event selection for the  $^{235}\text{U}$  uFC in Run 8. Horizontal scale in integrated codes. (a) Histogram of  $^{235}\text{U}$  uFC data after pedestal correction. (b) Histogram of remaining data after the pedestal peak was completely removed and a correction for missed events below the threshold was added. The orange band indicates the region of added events.

#### 5.4.2 Run 8 – $^{238}\text{U}$ data selection and correction

Pulse shapes of the 1000 individual events recorded for the  $^{238}\text{U}$  uFC in Run 8 have already been shown in Figure 9. The selection of pulses assigned as “good” fission events was done based on the pulse height spectrum (summed codes after base line subtraction) as shown in Figure 13. Note that unlike previous plots of this type, for this plot we have kept the negative polarity of the fission events. Two groups of events can be distinguished in Figure 13. One group forming a sharp peak at slightly above 0 integral value, and a broad distribution of events below about  $-2.5 \cdot 10^5$  integral value; the two groups are separated by a red vertical line in the figure. Events to the left of (below) the red line were identified as good fission events. There are **776** selected “good” fission events as shown in Figure 9a, and they display all the characteristics of properly recorded events.

The 224 discarded events are shown in Figure 9b. These pulses barely triggered a readout (note that the vertical scale extends only down to 0 codes) and have no proper base line. They are probably due to background in the rather harsh radiation environment around the operating neutron generator (such as alpha particles, gammas or x-rays) and, due to the quite widely fluctuating base line, mistakenly recorded with a pulse shape that only partly, or not at all,

contains the base line.

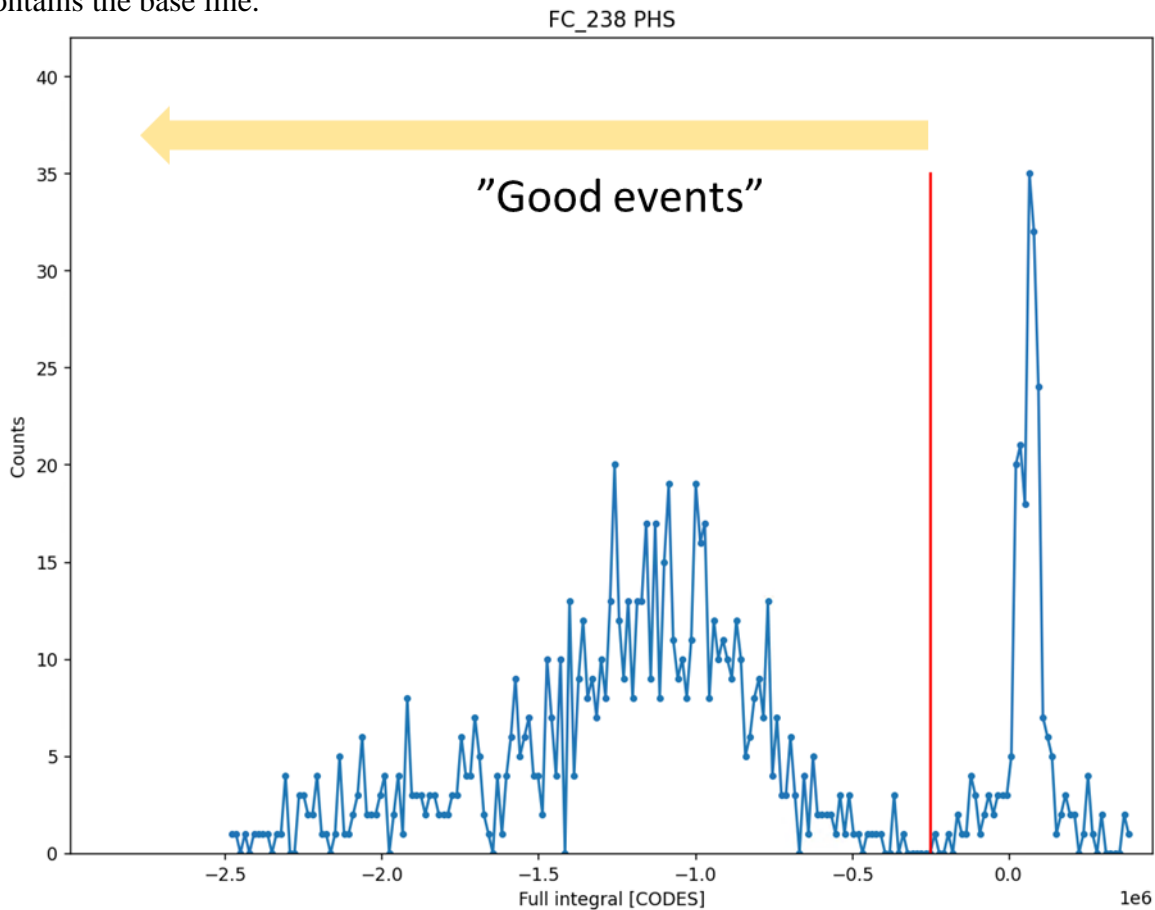


Figure 13. Pulse height spectrum of the 1000 events from the  $^{238}\text{U}$  uFC in Run 8. The pulse height integral is negative since it is based on a summing of code values of the original, negative polarity uFC pulses (after base line correction). Good fission events were selected as those falling to the left of the red line.

### 5.5 uFC background data

A 3-hour background run, with the neutron generator switched off, and with the uFC in the FCIB2 position and the LaBr detector remaining in its previous position, was conducted a few hours after the end of Run 8. A pulse height spectrum from this run for the  $^{235}\text{U}$  uFC is shown in Figure 14. The  $^{238}\text{U}$  uFC only gave 4 counts during the background run and is not further used in this analysis; LaBr background data is shown in Figure 15b below.

The  $^{235}\text{U}$  background data gives some guidance in interpreting the production run data from Run 7 and Run 8. Comparing the background distribution with Run 7 data (Figure 10a), it is clear that the shape and position of the pedestal peak largely agree with the peak observed in the background data. A scaled version of the background can be used to subtract from the production run data in order to provide a cleaner spectrum and help in the assessment of total number of good fusion events.

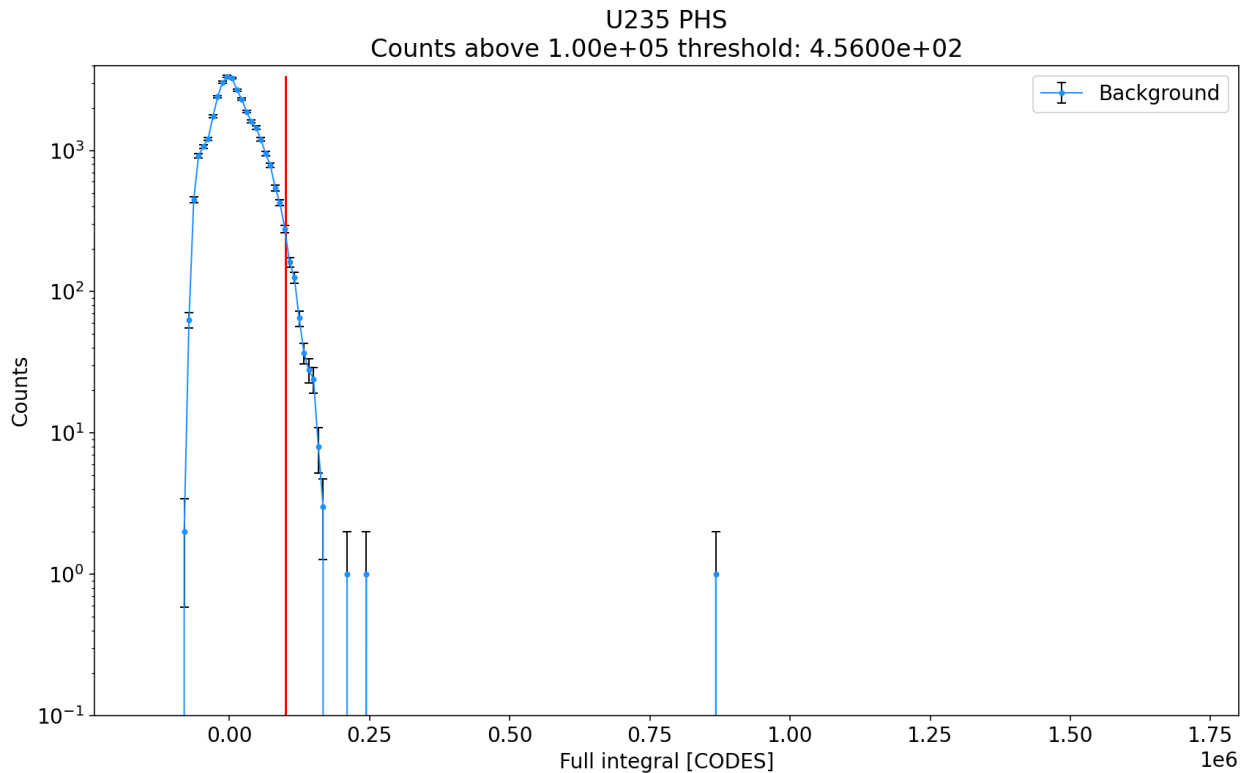


Figure 14. Pulse height spectrum for the  $^{235}\text{U}$  uFC in the Background run. The red vertical line indicates the software threshold used in the on-line neutron flux assessment.

### 5.6 Summary of count rate results

Combining the estimates of total number of good fission events earlier in this Section with the operating times given in Table 4 now allows for an estimate of the count rate in the two uFC in the two experimental positions. The data used for this calculation and the end result is given in Table 5.

**Table 5: Input data and resulting count rates for experimental Run 7 and Run 8.**

Run #	uFC location experiment	uFC coating	Data acquisition time (s)	Average neutron rate (n/s)	Experimental total nb counts <sup>(*)</sup>	Measured count rate (cps) <sup>(*)</sup>
7	CUP2	$^{235}\text{U}$	14400	$4.4 \cdot 10^8$	491955	<b>34.16</b>
7	CUP2	$^{238}\text{U}$	14400	$4.4 \cdot 10^8$	146852	<b>10.20</b>
8	FCIB2	$^{235}\text{U}$	73299 (**)	$1.8 \cdot 10^8$	162236	<b>2.213</b>
8	FCIB2	$^{238}\text{U}$	70456 (**)	$1.8 \cdot 10^8$	776	<b><math>11.01 \cdot 10^{-3}</math></b>

\* After correction for pedestal, background and events below threshold, as reported earlier in this Section.

\*\* Acquisition times differ slightly due the acquisition system crash and the fact that data buffers are only written to storage for every 100 events.

## 5.7 LaBr data

To complement the uFC in the determination of the (relative) neutron flux a LaBr scintillator detector was installed on a table in the NESSA outer bunker, viewing a block of paraffin blocking the collimator opening between the inner and outer bunkers. The detector was installed behind the thick wall separating the inner and outer bunkers thereby being shielded from direct illumination of neutrons from the generator. The block of paraffin was intended to moderate the high-energy component of the spectrum and possibly also give rise to characteristic gammas from neutron capture on hydrogen; however, this latter signal was not observed.

Pulse height spectra from the LaBr detector are shown in Figure 15, panel(a) from Run 7, panel (b) from the background run. The background data shows that a significant part of the Run 7 spectrum above a pulse height of about  $1.5 \cdot 10^6$  integrated codes is actually due to general background present in the NESSA bunker. We have for this analysis assumed that the background is stable in shape and present at an intensity proportional to the data accumulation time. A scaled version of Figure 15b has therefore been subtracted from the Run 7 and Run 8 LaBr data. The remaining events have been used to give a relative estimate of the time-resolved neutron flux, as further discussed below.

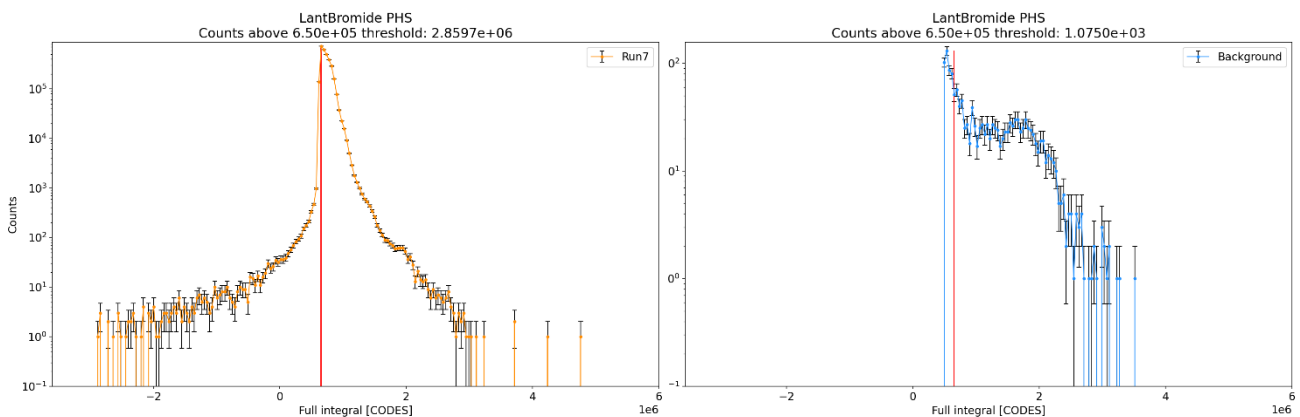


Figure 15. Pulse height spectra from the LaBr detector with a software threshold indicated by the vertical red line. (a) Run 7, (b) Background run.

## 6 Neutron transport calculations and estimated uFC count rates

Extensive neutron transport calculations were conducted as part of the safety case for the NESSA facility. The main purpose of these calculations was to assess the dose to the public in areas outside of the NESSA bunker system. However, several positions inside the NESSA bunker system were also included in these calculations, among them the so-called CUP1, a close user position at 17 mm from the source point, available for a neutron generator of different design than the one presently installed in the facility.

The calculations were done with the transport code MCNP, and the model used is graphically depicted in Figure 16. The outer dimensions of the NESSA radiation protection bunker shown in the figure are approximately  $4 \times 5 \text{ m}^2$ . The neutron flux calculated with this model for positions CUP1 and FCIB1 are shown in Figure 17. The calculations indicate that a reduction of about 4 orders of magnitude is expected for the direct flux around 14 MeV, while the scattered flux is only reduced by a bit more than one order of magnitude.

The MCNP calculated flux data can be used to estimate the count rate ( $C_R$  in counts per second) in the two uFC at the two locations from the formula:

$$C_R(\text{cps})_{i,\chi} = \varepsilon \cdot \sigma_{\text{average},i,\chi} \cdot N_i \cdot (nv)_{\chi} = S_i \cdot (nv)_{\chi} \quad (1)$$

where  $i$  =  $^{235}\text{U}$  or  $^{238}\text{U}$ , respectively,

$\chi$  = CUP2 or FCIB2, respectively,

$\varepsilon$  is the detection efficiency of the FC4A uFC,

$\sigma_{\text{average}}$  is the average cross section for flux  $i$  at position  $\chi$  [ $\text{cm}^2$ ]

$N$  is the number of uranium atoms in the detector [dimensionless],

and  $nv$  the energy-integrated neutron flux at position  $\chi$  (from MCNP) [ $\text{n}/(\text{s} \cdot \text{cm}^2)$ ]

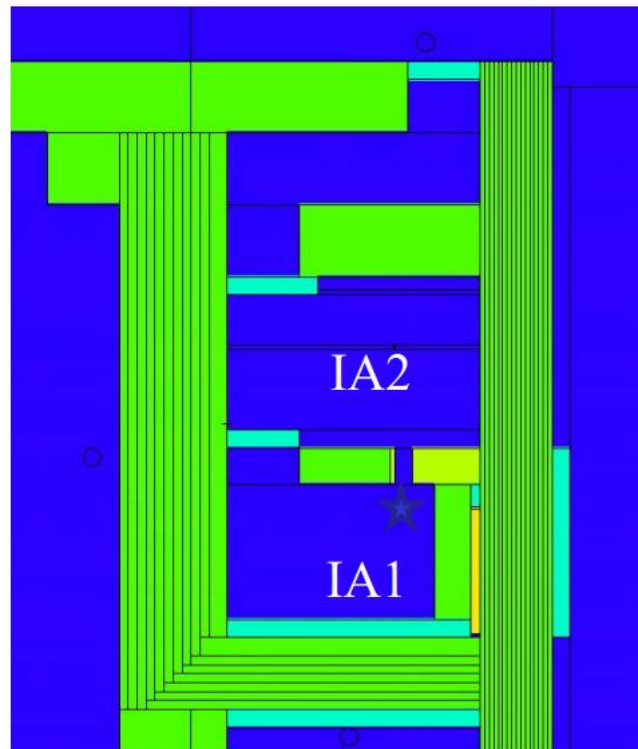


Figure 16. Graphical representation of the MCNP model used for neutron and gamma transport calculations for the NESSA safety case, top view of the facility. Dark blue is air, green is concrete, cyan is plastic, yellow-green is steel. The star indicates the position of the neutron generator. The footprint of the displayed area is about  $4 \times 5 \text{ m}^2$ .

### 6.1 Estimate of the uFC detection efficiency

Note that in equation (1), the quantity Sensitivity,  $S[\text{cm}^2] = \varepsilon \cdot \sigma_{\text{average},i,\chi} \cdot N_i$ , has been introduced. This is a quantity often quoted by fission chamber manufacturers and specific values provided by Centronic can be used to estimate the detection efficiency of their FC4A uFC. Note also that a quoted Sensitivity value is dependent on the spectrum of the neutron field and the number of uranium atoms in the detector, but independent of the intensity of the neutron flux.

In many cases, detection efficiencies of  $\varepsilon > 90\%$  are reported for fission chambers<sup>7,8</sup>. However, for chambers with thick coatings and tight geometry, effects like self-absorption and a curved geometry tends to lower the efficiency. In the case of the of the FC4A uFC the manufacturer<sup>9</sup> has indicated a detection efficiency of 60-70%.

In what follows we will estimate the FC4A detection efficiency based on data provided on the manufacturer's home page, combined with best estimates of average cross section and number of fissile nuclei in the deposit. Key to the evaluation are manufacturer data on the Sensitivity (Eq. 1) of the FC4A, namely a  $S_{th} = 3 \cdot 10^{-3}$  [cps/nv] for a thermal (Maxwellian) neutron spectrum at  $kT=25.3$  meV, and a  $S_{2.5} = 6.94 \cdot 10^{-6}$  [cps/nv] for mono-energetic neutrons at 2.5 MeV. As confirmed by Centronic, these Sensitivities apply to a FC4A with a “<sup>235</sup>U”-based deposit; here in quotation marks since the deposited fissile material is a mix of several uranium isotopes.

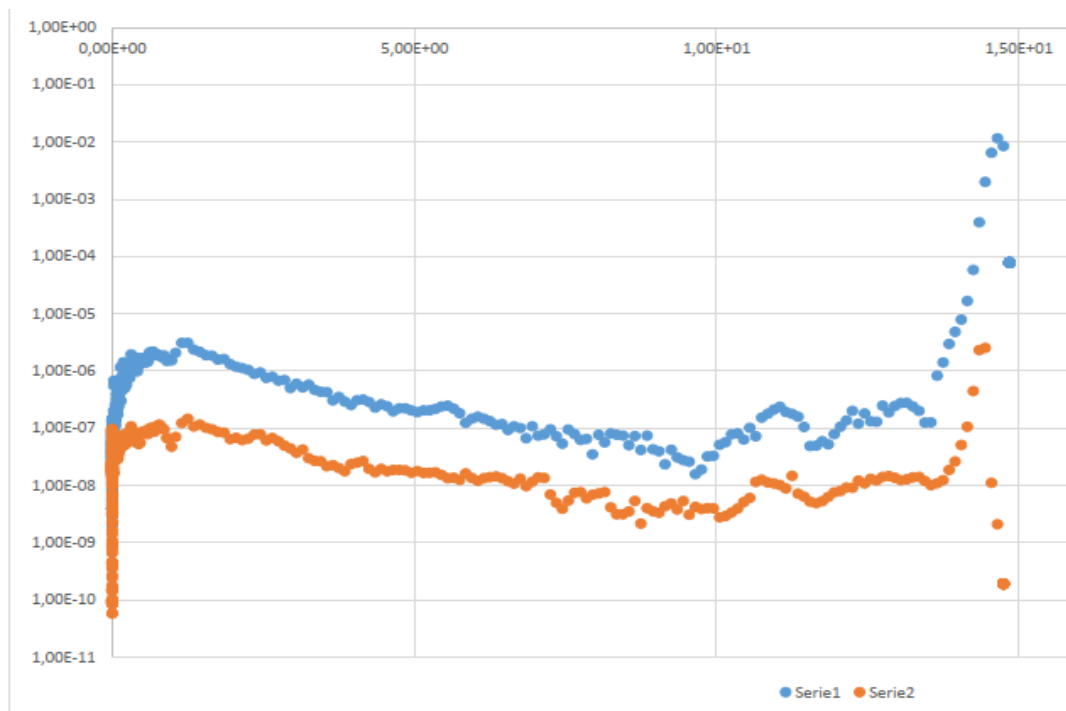


Figure 17. MCNP neutron flux calculation for the NESSA facility, positions CUP1 and FCIB1. The vertical scale gives the flux per bin per source neutron. The horizontal scale (shown at the top) gives neutron energy in MeV. Serie1 (blue dots) for the CUP1 position, Serie2 (orange dots) for the FCIB1 position. Note the double logarithmic scale.

The **number of uranium atoms,  $N$** , in the Centronic uFC chambers is calculated from the information provided from Centronic that a chamber deposit of  $M_{deposit} = 4$  mg concerns the amount of  $U_3O_8$ , introducing a factor  $f_U = (3 \cdot 235.04) / (3 \cdot 235.04 + 8 \cdot 16.0) = 0.84636$  as the weight fraction of uranium in the deposit. Furthermore, the data sheets provided with the delivery show that the “<sup>235</sup>U” chamber actually has a <sup>235</sup>U concentration of  $A_{235} = 93.177\%$  (by weight), a <sup>238</sup>U concentration of  $A_{238} = 5.38\%$ , and additionally small amounts of <sup>234</sup>U and <sup>236</sup>U at  $A_{234} = 1.011\%$  and  $A_{236} = 0.431\%$ . To simplify the calculations, we here make the approximation that the deposit contains only <sup>235</sup>U and <sup>238</sup>U, at concentrations  $A_{235} = 93.2\%$  and

<sup>7</sup> L.Mathieu et al., EPJ Web of Conferences 146, 03016 (2017)

<sup>8</sup> E.Provano et al., arXiv:2211.13323v2 (2022)

<sup>9</sup> M.Shaw (Exosens/Centronic Ltd), private communication, April 2026

$A_{238} = 6.8\%$ ; here  $^{238}\text{U}$  will represent all the even isotopes in the deposit. The atomic weights of  $^{235}\text{U}$  and  $^{238}\text{U}$  are  $m_{235} = 3.9030 \cdot 10^{-22}$  [g/atom] and  $m_{238} = 3.9508 \cdot 10^{-22}$  [g/atom] which gives the number of U atoms per 4 mg deposit as (approximately):

$$N_{235} = f_U \cdot A_{235} \cdot M_{\text{deposit}} / m_{235} = 0.84636 \cdot 0.932 \cdot 4 \cdot 10^{-3} / 3.9030 \cdot 10^{-22} = 8.0841 \cdot 10^{18}$$

$$N_{238} = f_U \cdot A_{238} \cdot M_{\text{deposit}} / m_{238} = 0.84636 \cdot 0.068 \cdot 4 \cdot 10^{-3} / 3.9508 \cdot 10^{-22} = 0.5827 \cdot 10^{18}$$

In the thermal case only the  $^{235}\text{U}$  component of the deposit contributes to the sensitivity (since the  $^{238}\text{U}(n,f)$  cross section is very small at these neutron energies), and the **Maxwellian average cross section (MACS)** for  $^{235}\text{U}$  in a thermal neutron field of temperature  $kT=0.0253$  eV can be directly read from, e.g., the JAEA home page<sup>10</sup>; it is stated to be  $\sigma_{\text{MACS},235} = 571.4$  [barn]. Note that this value includes an extra factor  $k = 2/\sqrt{\pi}$ .

Plugging in the values above in the expression (1) and solving for the efficiency,  $\varepsilon_{\text{th}}$ , gives:

$$\varepsilon_{\text{th}} = S_{\text{th}} / (\sqrt{\pi}/2 \cdot \sigma_{\text{MACS},235} \cdot N_{235}) = 0.003 / (0.88623 \cdot 571.4 \cdot 10^{-24} \cdot 8.0841 \cdot 10^{18}) = 0.7328$$

For the  $^{235}\text{U}$  chamber in a 2.5 MeV field both the  $^{235}\text{U}$  and the  $^{238}\text{U}$  (representing all even isotopes) components of the deposit contribute to the sensitivity, with their respective cross sections<sup>11</sup>:  $\sigma_{2.5,235} = 1.2615$  [barn],  $\sigma_{2.5,238} = 0.545$  [barn].

$$\varepsilon_{\text{th}} = S_{2.5} / (\sigma_{2.5,235} \cdot N_{235} + \sigma_{2.5,238} \cdot N_{238}) = 6.94 \cdot 10^{-6} / (1.2615 \cdot 10^{-24} \cdot 8.0841 \cdot 10^{18} + 0.545 \cdot 10^{-24} \cdot 0.5827 \cdot 10^{18}) = 0.660$$

There is some remaining uncertainty if the  $\sqrt{\pi}/2$  factor has possibly already been included in the stated value of  $S_{\text{th}}$ , which would bring down the  $\varepsilon_{\text{th}}$  to a value of 0.650, quite in line with the estimate of  $\varepsilon_{2.5}$ . In view of these uncertainties, in all subsequent calculations, the **detection efficiency,  $\varepsilon$** , of the Centronic FC4A uFC has been assumed to be the same for both types of chambers, i.e., both  $^{235}\text{U}$  and  $^{238}\text{U}$  deposit, with a (rounded off) value of  $\varepsilon = 0.65$ .

For the  $^{238}\text{U}$  chamber the isotopic purity is basically  $A = 1.00$  giving the number of  $^{238}\text{U}$  atoms:

$$N_{238}(^{238}\text{U uFC}) = f \cdot A \cdot M_{\text{deposit}} / m_{238} = 0.8480 \cdot 1.0 \cdot 4.0 \cdot 10^{-3} / 3.9508 \cdot 10^{-22} = 8.586 \cdot 10^{18}$$

## 6.2 Calculation of the average (n,f) cross section and neutron flux at CUP2 and FCIB2

The average fission cross section,  $\sigma_{\text{average},i,\chi}$ , for incident neutrons of a certain energy distribution is calculated using the MCNP calculated flux distributions and according to the standard averaging formula:

$$\sigma_{\text{average},i}(\phi_{\chi}(E)) = \int \frac{\phi_{\chi}(E) \sigma_i(E)}{\phi_{\chi}(E)} dE \quad (2)$$

where  $i$  =  $^{235}\text{U}$  or  $^{238}\text{U}$ , respectively,

$\chi$  = CUP2 or FCIB2, respectively,

$\phi_{\chi}(E)$  is the MCNP calculated energy-resolved neutron flux at position  $\chi$ ,

$\sigma_i(E)$  is the energy-resolved fission cross section for uranium isotope  $i$ .

<sup>10</sup> <https://www.ndc.jaea.go.jp/cgi-bin/Tab80WWW.cgi?lib=J40&iso=U235>

<sup>11</sup> JANIS data service, ENDF-VIII evaluation:

The  $^{235}\text{U}$  and  $^{238}\text{U}$  fission cross sections were retrieved in tabular form from the JANIS data base. The MCNP calculated neutron flux was obtained in the form of an Excel table. A linear interpolation in the cross-section table was used to obtain values for each calculated energy point in the flux data table. A numerical integration was performed to obtain the final average cross section value.

A complication in the present calculations is that the MCNP data were given for positions that slightly deviate, by a few cm, from the positions used in the experiments. This was taken into account by modifying the MCNP data (i.e., the  $\phi_\chi(E)$  table) in the following way.

The MCNP CUP1 position at 17 mm is about 2.35 times closer than the CUP2 position at 40 mm from the source point as used in the experiment; for the Genie16 generator this is the closest possible position for placing the uFC. This means that the direct flux ( $E_n > 13.0$  MeV) at the CUP2 position should be about a  $1/r^2$  factor  $f = 0.1806$  lower than that calculated for the CUP1 position. One can assume the low-energy, scattered flux to be almost the same for the CUP1 and CUP2 positions. Thus, a new  $\phi_{CUP1}(E)$  vector was calculated, where all  $\phi_{CUP1}(E)$  values for  $E_n > 13$  MeV were scaled by the factor  $f$ , and all  $\phi_{CUP1}(E)$  values for  $E_n < 13$  MeV were left unaffected.

Similarly, for the FCIB2 calculation we need to take into account the fact that the FCIB2 position is about 5 cm closer (at  $r = 130$  cm) to the neutron source point than the position used in the MCNP FCIB1 calculations (at  $r = 135$  cm). We have followed the recipe for the CUP above, assuming that the low-energy part of the spectrum is essentially unaffected by this relatively short shift and only considered an upshift of the flux for  $E_n > 13.0$  MeV by the  $1/r^2$  factor of  $g=1.0784$ .

With these modifications, the flux-averaged fission cross-sections were calculated using a numerical integration of Eq. 2, giving the following results:

$$\sigma_{average;235}(\phi_{CUP2}(E)) = 2.549 \text{ [b]}$$

$$\sigma_{average;238}(\phi_{CUP2}(E)) = 1.176 \text{ [b]}$$

$$\sigma_{average;235}(\phi_{FCIB2}(E)) = 92.27 \text{ [b]}$$

$$\sigma_{average;238}(\phi_{FCIB2}(E)) = 0.3698 \text{ [b]}$$

Finally, the neutron flux at the two measurement positions must be estimated. This is done from the MCNP calculation data in combination with the estimate of the source neutron rate from the Genie16 generator. Since the MCNP calculations are normalized to the flux per source neutron, the total neutron flux at the different positions  $\chi$ ,  $nV$  in equation (1), is simply given by the integral (numerical sum) over the MCNP flux vector multiplied with the generator rate,  $R$ :

$$nV_\chi = R_\chi \cdot \int \phi_{\chi(E)} dE \text{ [n/(s}\cdot\text{cm}^2\text{)]}$$

where  $R_\chi$  is the neutron generator source rate [n/s] for the measurement at position  $\chi$ .

With the approximate source rate in the two experiments given by the generator calibration as  $R_{CUP2} = 4.4 \cdot 10^8$  n/s and  $R_{FCIB2} = 1.8 \cdot 10^8$  n/s this results in the following values:

$$nV_{(CUP2)} = 2.37 \cdot 10^6 \text{ [n/(s}\cdot\text{cm}^2\text{)]}$$

$$nV_{(FCIB2)} = 1.02 \cdot 10^4 \text{ [n/(s}\cdot\text{cm}^2\text{)]}$$

### 6.3 Calculation of uFC expected count rates at CUP2 and FCIB2

We are now in a position to use the formula (1) for the four different combinations of uFC and measurement positions to calculate the expected absolute count rates.

Here it should be noted that according to the delivery data sheets, the “<sup>235</sup>U chamber” actually contained 4.4 mg of U<sub>3</sub>O<sub>8</sub> deposit. The data sheets gave the weight of deposit for the <sup>238</sup>U chamber as “4000 g”, i.e., exactly the nominal amount. The 10% increase in material in the “<sup>235</sup>U chamber” has been taken into account in the calculations below.

For the CUP2 position:

$$C_{R,235} = 4.4/4 \cdot \varepsilon \cdot (\sigma_{\text{average},235,\text{CUP2}} \cdot N_{235} + \sigma_{\text{average},238,\text{CUP2}} \cdot N_{238}) \cdot (nV)_{\text{CUP2}} =$$

$$1.1 \cdot 0.65 \cdot (2.549 \cdot 10^{-24} \cdot 8.0841 \cdot 10^{18} + 1.176 \cdot 10^{-24} \cdot 0.5827 \cdot 10^{18}) \cdot 2.37 \cdot 10^6 = 36.1 \text{ [cps]}$$

$$C_{R,238} = \varepsilon \cdot \sigma_{\text{average},238,\text{CUP2}} \cdot N_{238} \cdot (nV)_{\text{CUP2}} = 0.65 \cdot 1.176 \cdot 10^{-24} \cdot 8.586 \cdot 10^{18} \cdot 2.37 \cdot 10^6 = 15.5 \text{ [cps]}$$

For the FCIB2 position:

$$C_{R,235} = 4.4/4 \cdot \varepsilon \cdot (\sigma_{\text{average},235,\text{FCIB2}} + \sigma_{\text{average},238,\text{FCIB2}} \cdot N_{238}) \cdot N_{235} \cdot (nV)_{\text{FCIB2}} =$$

$$1.1 \cdot 0.65 \cdot (92.27 \cdot 10^{-24} \cdot 8.0841 \cdot 10^{18} + 0.3698 \cdot 10^{-24} \cdot 0.5827 \cdot 10^{18}) \cdot 1.02 \cdot 10^4 = 2.22 \text{ [cps]}$$

$$C_{R,238} = \varepsilon \cdot \sigma_{\text{average},238,\text{FCIB2}} \cdot N_{238} \cdot (nV)_{\text{FCIB2}} = 0.65 \cdot 0.3698 \cdot 10^{-24} \cdot 10.12 \cdot 10^{18} \cdot 1.02 \cdot 10^4 = 8.60 \text{ [mcps]}$$

## 7 uFC count rates: Summary of results and discussion

The numerical results from the previous sections are summarized in Table 6. For reference, also calculated count rates for 100% efficient uFC are included. In the table is also reported the ratio  $F = C_{R(235)}/C_{R(238)}$  between the count rate estimates in the two uFC, both for the experiment and for the MCNP calculations.

There is a good agreement between the observed, experimental count rates and the calculated, absolute count rates (entries marked in red in the table). This is particularly true for the results for the <sup>235</sup>U uFC for which the calculated count rates deviate from the measured ones by less than 6%, for both the CUP2 and FCIB2 positions, respectively. For the <sup>238</sup>U uFC, the difference between experiment and calculation is larger, with the calculated result in CUP2 deviating by +52% and the result for the FCIB2 position deviating by -22%.

A proper uncertainty analysis of these data has not been done at this moment. One can note, however, that counting statistics is in general good, with the smallest event sample being that from the <sup>238</sup>U uFC in the FCIB2 position, where a total of 776 events were recorded as good fission events; this gives a statistical uncertainty of about 3.5%; for the other data sets the statistical uncertainty is on the few permille level. The largest uncertainty is probably due to event selection and corrections, where in particular the data from the <sup>238</sup>U uFC in the CUP2 position poses some problems. It might well be that in that case, the hardware threshold is active at a (much) higher level (in integrated codes) than estimated here. This would tend to increase

the correction for events lost below the threshold, thereby also increasing the count rate estimate from the present 10.2 cps to something higher. It is worth noticing that this data point is also the one deviating from the calculated estimates the most.

**Table 6: Results from measurements and calculations.**

Run #	uFC location experiment	uFC coating	Measured count rate (cps)*	Calculated count rate ( $\epsilon=100\%$ )	Calculated count rate ( $\epsilon=60\%$ )	CR ratio exp (235/238)	CR ratio calc (235/238)
7	CUP2	$^{235}\text{U}$	<b>34.16</b>	65.61	<b>36.1</b>	3.21	2.32 $\pm 0.7^{**}$
7	CUP2	$^{238}\text{U}$	<b>10.20</b>	26.51	<b>15.55</b>		
8	FCIB2	$^{235}\text{U}$	<b>2.213</b>	4.04	<b>2.24</b>	189	259 $\pm 73^{**}$
8	FCIB2	$^{238}\text{U}$	<b><math>11.01 \cdot 10^{-3}</math></b>	$15.60 \cdot 10^{-3}$	<b><math>8.60 \cdot 10^{-3}</math></b>		

\* After correction for background, pedestal and events below threshold

\*\* Error in the ratio from a rough, estimated uncertainty in the cps values of 20%

In general, these results tend to support the MCNP results (on dose to the public outside of the NESSA bunker) produced for the NESSA safety case, and could be used in future communications with the radiation authorities for reporting; tentatively, they verify the proper design of the NESSA radiation protection bunker.

## 8 Neutron generator source stability

The neutron monitoring system based on the two uFC described here was designed for a neutron generator providing a rate of about  $10^{10}$  n/s. With the present Sodern Genie16, source rates of up to  $4.5 \cdot 10^8$  n/s can be achieved. This in combination with the rather distant closest user position (the CUP2 at 40 mm extensively used in this report) gives a situation where count rates in the uFC are quite modest. Therefore, using the uFC system for any more detailed monitoring of the short-term variations in neutron generator source strength is not possible at present. In order to give some further insights into this issue, the uFC were complemented by a LaBr scintillator, placed out of direct sightline from the generator. The scintillator nevertheless gave a quite high count-rate of scintillation events, due to the abundant ambient radiation of neutrons, gammas and x-rays present in the rather harsh environment around the operating neutron generator.

Despite the limitations described above, a comparison between the  $^{235}\text{U}$  uFC time-resolved count rate and that of the LaBr detector can give some indications of possible source strength variations over time. In Figure 18 we compare the count rate evolution of the  $^{235}\text{U}$  uFC and the LaBr detector over the 4 hours of Run 7. The uFC had an average count rate of 30.8 events/s, while the LaBr counted at around 158 counts/s. This difference has led to the different time

bases used in the panels of Figure 18.

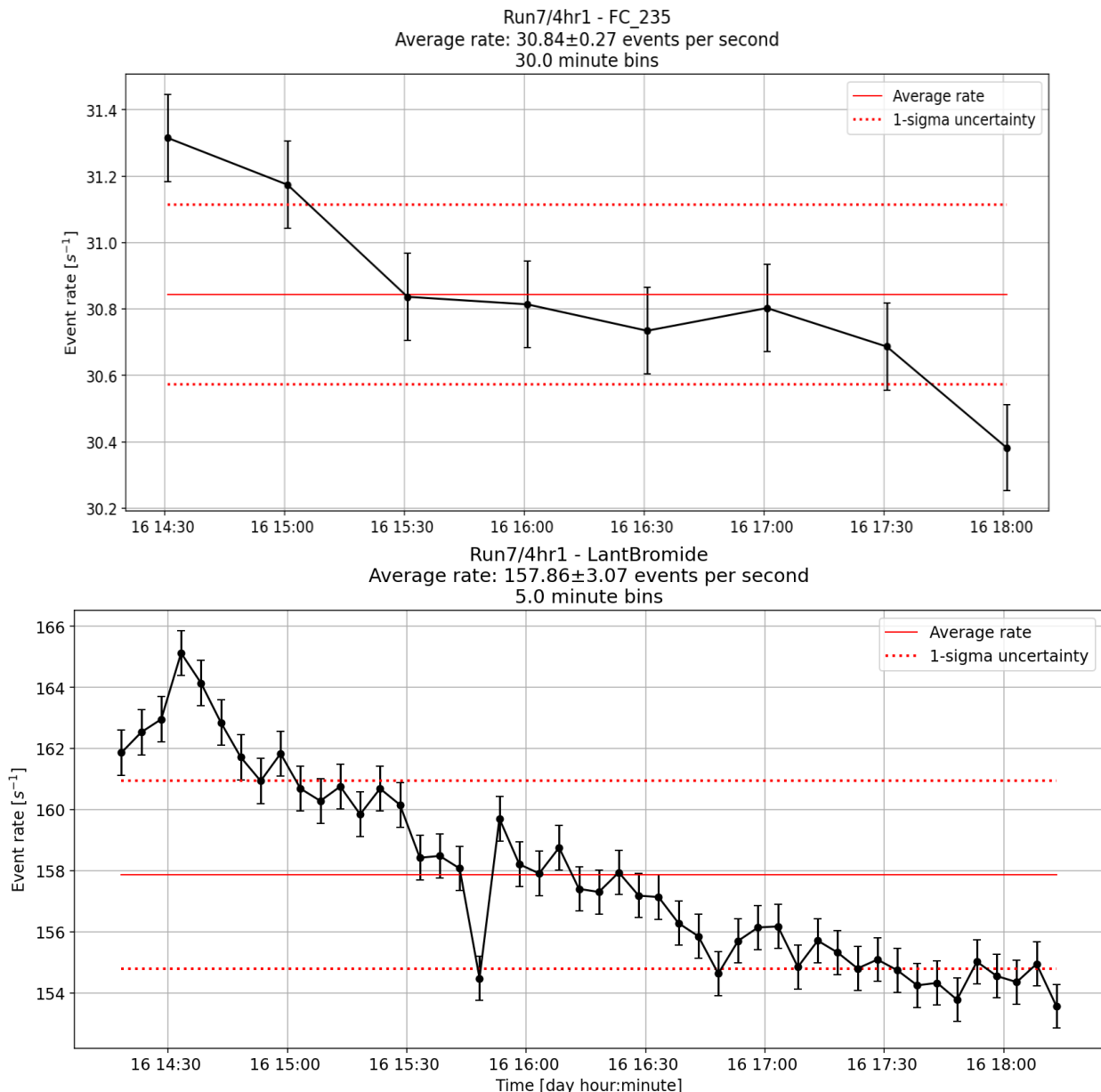


Figure 18. Comparison of time-evolution of count rates in the  $^{235}\text{U}$  uFC and the LaBr scintillator during the 4 hours of Run 7. The two panels have been roughly aligned to facilitate a comparison.

Over the 4 hours of Run 7, the count rate in the  $^{235}\text{U}$  uFC dropped by about 3%, when comparing the first data point with the last. Over the same period the LaBr detector displayed a similar trend, decreasing in rate by about 7%. This agreement seems to suggest there may have been a small decrease in neutron generator source strength over the 4 hours of Run 7. The larger drop in LaBr count rate can possibly be due to a small drift in amplification of the photo-multiplier tube attached to the LaBr scintillation crystal. Pulse height spectra from the LaBr detector corroborates this idea, although further investigations are required to make any more firm statement.

It can be added that the electrical operating parameters of the neutron generator over this time were perfectly stable.

## 9 Summary and conclusions

The neutron monitoring system for the NESSA neutron irradiation facility was procured, tested, installed and commissioned in 2025 – 2026. The system is based on a pair of micro fission chambers (uFC) procured from Centronic Ltd, UK (now Exosens). In particular, a dedicated set of experiments using a Sodern Genie16 neutron generator were conducted in February 2026 to study the count rates and long-term behavior of the uFC in operations close to the maximum rate of the generator, at  $4.5 \cdot 10^8$  n/s. The system performed as intended, and showed that long-term operations of the detectors is possible; in this case the monitoring system was operated continuously for about 3 days.

In these experiments the uFC were exposed to the neutron field around the generator in two different positions for which extensive MCNP calculations had been performed as part of the NESSA safety case. Comparisons of the experimental and calculated count rates (the latter based on MCNP calculations, Uranium cross section data and the amount of fissile material in the uFC) showed good agreement, well within 10% for the  $^{235}\text{U}$  uFC and within about 50% for the  $^{238}\text{U}$  uFC.

These results tend to corroborate the dose calculations filed as part of the NESSA safety case and can be used in communications with authorities, when reporting the operational status of NESSA.

## 10 Acknowledgements

We are grateful to the Carl Trygger Foundation for the financial support that has made this development possible.

## 11 APPENDIX

Items included in the neutron rate monitoring system are listed in the table below. All items in the list, except for the  $^{238}\text{U}$  uFC, were procured from the grant from the Carl Trygger Foundation.

**Table:** List of items included in the NESSA neutron rate monitoring system, specifying some minor details for the purpose of reporting a procurement grant from the Carl Trygger Foundation. Items NOT procured under the Carl Trygger Foundation grant are indicated in italics.

Item	Company	Cost (SEK)
ADQ14 4-channel digitizer, 1 GSPS, 14 bit	Teledyne SP Devices	- 107 394
National Instruments: 1x 9-slot PXIe chassis, 1x PXIe Widows 6-core controller	C N Rood	- 97 465
MPR-1: 2x pre-amplifier	Mesytec	- 26 779
Low voltage distributor NIM 4-channel	Mesytec	- 10 789
Centronic: 1x 235-U micro- fission chamber	Centronic/Exosens	- 102 683
<i>Centronic: 1x 238-U micro- fission chamber</i>	<i>Centronic/Exosens</i>	
Caen: 1x 4-channel high voltage unit	Gammadata	- 74 000
Misc. components (adapters, connectors) from RS components, Amerikanska tel, Farnell	RS Components+	- 4 159
PC for the data acquisition system	Dell	- 7 345
Adapter (HN to BNC adapter for uFC)		- 1 344
Computer components (monitor)	Dell	- 3 514
Shipping (transport of neutron generator Lund-Uppsala)		- 18 200
University overhead (max allowed by CTS SEK48180:-)		- 26 675
Not used		5 833
Total grant:		486 180